



HAL
open science

Synthesis, structural characterisations, NMR spectroscopy, Hirshfeld surface analysis and electrochemical study of a new organic cyclohexaphosphate, (C 6 H 7 FN) 4 (Li) 2 (P 6 O 18) (H 2 O) 6

A. Hamdi, L. Khedhiri, M. Kahlaoui, S. Soudani, V. Ferretti, Fabrice Lefebvre, Christian Jelsch, E. Wenger, C. Ben Nasr

► **To cite this version:**

A. Hamdi, L. Khedhiri, M. Kahlaoui, S. Soudani, V. Ferretti, et al.. Synthesis, structural characterisations, NMR spectroscopy, Hirshfeld surface analysis and electrochemical study of a new organic cyclohexaphosphate, (C 6 H 7 FN) 4 (Li) 2 (P 6 O 18) (H 2 O) 6. *Journal of Molecular Structure*, 2018, 1170, pp.30-37. 10.1016/j.molstruc.2018.05.062 . hal-02365367

HAL Id: hal-02365367

<https://hal.science/hal-02365367>

Submitted on 16 Feb 2022

HAL is a multi-disciplinary open access archive for the deposit and dissemination of scientific research documents, whether they are published or not. The documents may come from teaching and research institutions in France or abroad, or from public or private research centers.

L'archive ouverte pluridisciplinaire **HAL**, est destinée au dépôt et à la diffusion de documents scientifiques de niveau recherche, publiés ou non, émanant des établissements d'enseignement et de recherche français ou étrangers, des laboratoires publics ou privés.

Published in *Journal of Molecular Structure*, 2018, 1170, 30-37.

<https://doi.org/10.1016/j.molstruc.2018.05.062>

**Synthesis, structural characterisations, NMR Spectroscopy, Hirshfeld
Surface Analysis and electrochemical study of a New Organic
Cyclohexaphosphate, $(C_6H_7FN)_4(Li)_2(P_6O_{18})(H_2O)_6$**

A. Hamdi^a, L. Khedhiri^a, M. Kahlaoui^b, S. Soudani^a, V. Ferretti^c, F. Lefebvre^d, C. Jelsch^e, E.

Wenger^e, C. Ben Nasr^{a*}

^a Laboratoire de Chimie des Matériaux, Faculté des Sciences de Bizerte, 7021 Zarzouna, Université de Carthage, Tunisie.

^b Unité de service commun spectromètre de surfaces, Faculté des Sciences de Bizerte, Université de Carthage, Zarzouna 7021, Tunisia.

^c Department of Chemical and Pharmaceutical Sciences and Center for Structural Diffraction, via Fossato di Mortara 17, I-44121 Ferrara, Italy

^d Laboratoire de Chimie Organométallique de Surface (LCOMS), Ecole Supérieure de Chimie Physique Electronique, 69626 Villeurbanne Cedex, France.

^e CRM², CNRS, Institut Jean Barriol, Université de Lorraine, Vandoeuvre les Nancy CEDEX, France.

Abstract

$(C_6H_7FN)_4(Li)_2(P_6O_{18})(H_2O)_6$ (**I**), a new organic cyclohexaphosphate, has been synthesized and grown at room temperature by an acid/base reaction between $H_6P_6O_{18}$ and 2-fluoroaniline as an organic template. The crystal structure of (**I**) was solved by single crystal X-ray diffraction analysis and it was found that the material belongs to triclinic system with space group P-1 and refined *R*-factor of 0.0520. Adjacent P_6O_{18} rings are connected via corner-sharing by LiO_4 tetrahedra, generating anionic $[Li_2P_6O_{18} \cdot H_2O]^{4-}$ layers parallel to the (**a**, **b**) plane. The 2-fluoro-anilinium cations are inserted in the interlayer space and interact with the

inorganic framework through N-H...O and O-H...O hydrogen-bonding interactions. Additional stabilization is provided by strong N-H...F and weak C-H...O hydrogen bonds. Hirshfeld surface analysis reveals the nature of intermolecular contacts of the title compound and their enrichment ratio reveals if they are over-represented. The crystal packing is a combination of strong electrostatic attractive interactions and of weaker hydrophobic contacts. The title compound was further characterized by FT-IR and NMR spectroscopies. Crystal symmetry is confirmed by ^{31}P magic angle spinning NMR and the vibrational absorption bands were identified by infrared spectroscopy. Electrical conductivity was studied using impedance spectroscopy and results showed that the conductivity at 150°C was equal to $4.93 \times 10^{-4} \text{ S.cm}^{-1}$. It is therefore concluded that $(\text{C}_6\text{H}_7\text{FN})_4(\text{Li})_2(\text{P}_6\text{O}_{18})(\text{H}_2\text{O})_6$ can be further used in lithium batteries.

Keywords: Cyclohexaphosphate ; Hirshfeld surface ; Contacts enrichment ; ^{31}P MAS-NMR; Infrared spectroscopy ; conductivity.

1. Introduction

Much attention has been devoted to the synthesis of open-framework phosphates which exhibit a rich structural diversity and have been widely studied as catalysts, ion-exchangers and as positive electrode in lithium and sodium batteries [1]. Within this family of compounds, the resulting anionic frameworks, generally constructed from PO_4 tetrahedra that are vertex linked with MO_n polyhedra, generate pores and channels offering suitable environment to accommodate different other cations.

Cyclophosphates are characterized by a cyclic $(\text{PO}_3^-)_n$ anion built by n corner-sharing PO_4 tetrahedra. Ring anions of this type are presently well characterized for $n = 3, 4, 5, 6, 8, 10$ and 12. For each family of cyclophosphates, corresponding to a particular value of n , the methods of chemical preparation are very specific and with few exceptions, the development

of these methods required the optimization of a procedure for the chemical preparation of an appropriate starting material.

There is considerable scientific and technological interest in the synthesis, structure and properties of cyclohexaphosphates ($n = 6$) because these compounds offer high hydrolytic and thermal stability and pronounced complexation ability. In particular, cyclohexaphosphates were shown to be potentially attractive as precursors in the solid state synthesis of simple and mixed-cation polyphosphates for glass making [2, 3].

It has been found that the hydrogen bonds and the nature of organic molecules seem to determine the molecular organization of these compounds as to built infinite anionic networks with various geometries: ribbons [4], two-dimensional networks [5-7] and three dimensional network [8, 9].

This paper relates a contribution to the study of cyclohexaphosphates including organic-monovalent cations. Up to now, few examples of this type of compound are reported [10-13]. Here, we report on the synthesis of a new cyclohexaphosphate with formula $(C_6H_7FN)_4(Li)_2(P_6O_{18})(H_2O)_6$ (**I**). This latter is further characterized by IR and NMR spectroscopies. The electrical properties of the above mentioned material and its comparison to other results were studied.

2. Experimental

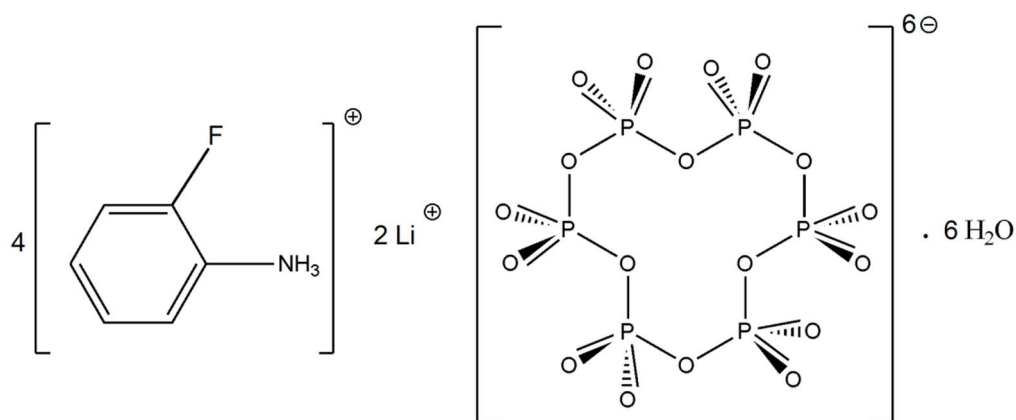
2.1. Chemical Preparation

The title compound $(C_6H_7FN)_4(Li)_2(P_6O_{18})(H_2O)_6$ (**I**) was prepared by an acid-base reaction between the 2-fluoroaniline, purchased from Sigma-Aldrich, and the cyclohexaphosphoric acid. An aqueous solution (10 mL) of $H_6P_6O_{18}$ (2 mmol) was first prepared by passing a solution of $Li_6P_6O_{18}$ through an ion exchange resin (Amberlite IR120) in

its H-state. The Lithium salt $\text{Li}_6\text{P}_6\text{O}_{18}$ was produced according the process described by Schülke [14]. The cyclohexaphosphoric acid is cooled and neutralized by adding slowly 2-fluoroaniline (8mmol) dissolved in 5mL of ethanol which is supplied by Novachim. The resulting solution is then slowly evaporated over few days at ambient temperature to give large rectangular prisms of stable crystals of the title compound.

The lithium existence in **(I)** resulted from an incomplete Li^+/H^+ exchange of $\text{Li}_6\text{P}_6\text{O}_{18}$ on the used resin.

Schematically the reaction can be written:



(I)

2.2. X-Ray Single Crystal Structure Analysis

The crystallographic data were collected on a D8 Venture Bruker diffractometer at room temperature using mirror-monochromated $\text{MoK}\alpha$ radiation ($\lambda = 0.71073 \text{ \AA}$). Data sets were integrated with the Bruker APEX Suite [15] and corrected for Lorentz-polarization and absorption effects [16]. The structure was solved by direct methods (SIR97) [17] and refined by full-matrix least-squares methods with all non-hydrogen atoms anisotropic. Hydrogens of the methyl groups were included on calculated positions, riding on their carrier atoms. All other

hydrogen atoms were located in the difference-Fourier map and refined isotropically. All calculations were performed using SHELXL-2014/7 [18] implemented in the Olex program [19]. Some data collection parameters and results of the structure determination are given in **Table 1**. Selected bond distances and angles are given in **Table S2** and **Table 2**. The drawings were made with Diamond [20].

2.3. NMR and IR measurements

The NMR powder spectra were recorded on a solid-state high-resolution Bruker Avance-500 spectrometer operating at 125.81 MHz for ^{13}C , 50.50 MHz for ^{15}N , 470.38 MHz for ^{19}F and 202.51 MHz for ^{31}P with a classical 4 mm BB/1H dual MAS probe allowing spinning rates up to 10 - 14 kHz. The ^{13}C , ^{15}N and ^{31}P NMR spectra were recorded by using cross-polarization (CP) and decoupling from protons (contact time 2 ms) while the ^{19}F spectrum was obtained by direct irradiation. Before recording the spectra, it was checked that there was a sufficient delay between the scans allowing a full relaxation of the protons, typically 30 s in the present case. A ^{31}P NMR spectrum was also recorded by direct irradiation and proton decoupling (recycle delay 100 s) and did not show any difference with that recorded by CP. ^{13}C , ^{15}N , ^{19}F and ^{31}P NMR chemical shifts are given relative to external tetramethylsilane, neat nitromethane, fluorotrichloromethane and 85 wt. % phosphoric acid, respectively (precision 0.5 ppm). For ^{31}P , the isotropic chemical shift values (δ_{iso}) of the three NMR species were determined from the position of the peaks that did not change in the spectra taken with different spinning rates. The analysis of the ^{31}P MAS-NMR spectrum was carried out by using the Bruker program WINFIT [21]. The intensities of the side bands were computed by the method of Herzfeld and Berger [22]. Chemical shift anisotropy ($\Delta\delta_{\text{CS}}$) and the asymmetric parameter (η) of NMR components were then determined (**Table 3**). The IR spectrum was recorded in the 4000-400 cm^{-1} range using a NICOLET IR 200 FT-IR infrared spectrometer.

2.4. Electrical measurements

The $(\text{C}_6\text{H}_7\text{FN})_4(\text{Li})_2(\text{P}_6\text{O}_{18})(\text{H}_2\text{O})_6$ cyclohexaphosphate powder was ground in an agate mortar and then pressed at 3 Tons into cylindrical pellet with 12.7 mm in diameter and 1.5 mm in thickness.). Complex impedance spectra were obtained using a Hewlett-Packard HP 4192 analyzer. The impedance measurements were taken in an open circuit using two electrode configurations with signal amplitude of 0.5V and a frequency band ranging from 10 Hz to 13MHz. Both pellet surfaces were coated with silver pastes electrodes while the platinum wires attached to the electrodes were used as current collectors. Measurements were performed at equilibrium potential at a temperature ranging between 75°C and 150°C. In order to obtain the conductivity, the resulting data was analyzed using the equivalent circuit of the Z-View software.

3. Results and Discussion

3.1. Structure description

The structural formula of **(I)** includes various entities: one phosphoric ring lying on an inversion center $(0, \frac{1}{2}, \frac{1}{2})$, two lithium atoms, six water molecules out of which four are coordinated to the Li atoms and four 2-fluoroanilinium cations. The geometrical configuration of these species is depicted in **Fig. 1**.

Through corner sharing, the phosphoric rings are linked by lithium atoms and water molecules generating a two dimensional inorganic framework extending along the **(a, b)** plane as shown in **Fig. S1**.

The P_6O_{18} ring anion is formed by three independent PO_4 tetrahedra and adopts a chair conformation. The geometric features of the phosphoric ring (P-O and O-O distances, O-P-O and P-O-P angles) are reported in **Table S1**, whereas the calculated average values of their

distortion indices (DI) [23] are illustrated in **Table S2**. The P-O distances range from 1.4535(2) to 1.6061(2) Å with an average of 1.532 Å. In spite of these differences in P-O bond lengths, which can be explained by different environments of the O atoms, each PO₄ tetrahedron can be described by regular oxygen atoms arrangement with phosphorus atom shifted of 0.117, 0.132, 0.148 Å from the gravity centre (**Table S2**). Furthermore the DI(PO) = 0.039, DI(OPO) = 0.037 and DI(OO) = 0.012 (**Table S2**) values show an above distortion of the O-O distances compared to P-O ones. The P-O-P angles values correspond to those generally observed in similar cyclohexaphosphates [24, 25], with the exception of the P1-O4-P2 angle of 141.50(1)°, significantly different from the value generally observed in such anions; this angle is associated with the longest P1-P2 distance (2.991(3) Å). It should be noted that these values display the greatest divergence observed so far. The P-P-P angles, ranging from 96.40(3) to 109.37(3) ° and with an average value of 104.62°, show that the rings are significantly distorted from the ideal three-fold symmetry. In spite of this variance, the distortion is less important if compared with that observed in (C₈H₁₂N)₄(Li)₂(P₆O₁₈)(H₂O)₆ [26], in which the average of the P-P-P angle is 107.05°.

Fig. S2 and Fig. 2 exhibit the complete atomic arrangement of the structure projected along the *b* and *a*-axis respectively. These projections show that the packing of (**I**) consists of two hybrid layers: the first one, made of inorganic [Li₂P₆O₁₈·H₂O]⁴⁺ hetero-anions, is developed parallel to the (a, b) plane around *z* = ½, while the second one, made of organic [C₆H₇N]⁺ cations, is inserted in the space between the inorganic layers.

The two independent 2-fluoroanilinium cations (**Fig. S3**) have (N-C, C-C) bond lengths and (N-C-C, C-C-C) bond angles in the range 1.346(9)-1.528(4) Å and 108.4(3)-124.6(4)°, respectively, (**Table 2**) that agree well with those observed in similar cyclohexaphosphates such as in [p- (F) C₆H₄NH₃]₆P₆O₁₈ ·2H₂O [27]. The cations are anchored onto successive layers through medium/strong H-bonds involving the hydrogen atoms of the -NH₃ groups, water

molecules and some external oxygen atoms of the P_6O_{18} groups with N(O)...O(E,W) distances varying between 2.688(4) and 3.202(4) Å and H...O(E,W) distances ranging between 1.87(4) and 2.31(4) Å. In addition, a number of stronger N-H...F and weaker C-H...O(E) interactions, listed in **Table S3**, are observed. The two hydrogen atoms of the water molecule O(W2) act as a link between successive anions.

The lithium atoms present a tetrahedral coordination as well, being coordinated to two water molecules O(W) and two O atoms O(E) belonging to two $P_6O_{18}^{6-}$ ring anions (**Fig. S1**). The geometrical features of the LiO_4 tetrahedron show that it is as regular as the PO_4 tetrahedra, being slightly distorted with Li-O distances ranging from 1.890(4) to 2.000(4) Å (**Table S1**). The smallest distance between two tetrahedral centers is 5.649 (1) Å.

3.2. Crystal contacts

The Hirshfeld surface was generated using MoProViewer [28] around the different entities of the $(C_6H_7FN)_4Li_2(P_6O_{18})(H_2O)_6$ formula. The enrichment ratios [29] of contacts between the different chemical species were computed in order to highlight which contacts are favored and are likely to be the crystal driving force.

Globally, hydrogen constitutes the first chemical species (40%) present on the Hirshfeld surface, followed by oxygen and carbon (**Table 3**). The Ho/n...O strong hydrogen bonds involving the cyclohexaphosphate, the water and the NH_3^+ group are the most abundant interaction type and are enriched at $E=2.2$ (**Fig. 3**). The weak Hc...O hydrogen bonds are only slightly enriched due to competition with the Hn/o...O and Li...O stronger interactions. The lithium cation is mostly interacting with oxygen atoms. The P...Hn/o contacts are presumably enriched due to the proximity with P-O...H-O-H hydrogen bonds.

Hydrophobic contacts are also important in the structure, as the C...C contact is the most enriched due to systematic $\pi... \pi$ stacking between the two independent fluoro-aniline moieties.

The fluorine atom forms mostly hydrophobic contacts with C and Hc atoms. The C...Hc interactions are enriched while Hc^{δ+}...Hc^{δ+} contacts are slightly under-represented as they are less favorable from an electrostatic point of view. The two fluoro-aniline molecules have similar environments as their contacts proportions C_{xy} show a correlation of 89%. **Figure 3** shows the second fluoro-aniline molecule with the NH₃⁺ group forming three hydrogen bonds with oxygen atoms of the cyclohexaphosphate, following a three-fold pseudo-symmetry. The NH₃⁺ group of the other organic cation interacts, on the other hand, with three different cyclohexaphosphate anions.

3.3. HOMO-LUMO Analysis

The frontier molecular orbitals, HOMO and LUMO, are the most important orbitals for determining the way the molecules interact with other species. The energy gap between HOMO and LUMO is a critical parameter to determine the charge transfer process within the molecule. HOMO-LUMO orbitals were calculated from the crystal data with the B3LYP/6-31+G* method and the Gaussian 09 program [30] and are displayed in **Fig. S5**. The highest occupied molecular orbital (HOMO) is located mainly around the phosphoric rings which behaves as an electron donor with a calculated energy of -3.15 eV, while the lowest unoccupied molecular orbital (LUMO) is concentrated on the NH₃ group of one 2-fluoroanilinium cations which behaves as an electron acceptor (calculated energy of LUMO is -2.979 eV). The energy gap between the HOMO and LUMO orbitals is 0.836 eV, a value which is relatively small suggesting that the title compound is kinetically slowly stable and has a high chemical reactivity because it is energetically favorable to add electron to a high-lying LUMO and to extract electrons from low-lying HOMO [31]. The energy distribution of the different orbitals for the synthesized compound is shown in **Fig. S6**.

3.4. Molecular Electrostatic Potential analysis (MEP)

The molecular electrostatic potential of the title compound has been computed at the B3LYP/6-31+G* level and is shown in **Fig. 4**. The molecular electrostatic potential (MEP) is used to predict the molecular reactive behavior towards electrophilic and nucleophilic attack and defined sites of the electrophile and nucleophile. The electrostatic potential maps are color-coded and are subdivided into many regions where those various colors are used to identify different potentials. Intermediate potentials are assigned colors according to the following color spectrum: red < orange < yellow < green < blue. As seen from **Fig. 4**, the positive region is localized on the lithium atoms while the negative region is located on the oxygen of the phosphoric rings and the green regions are located around the organic cations.

3.5. NMR results

The ^{13}C CP-MAS NMR spectrum of $(\text{C}_6\text{H}_7\text{FN})_4(\text{Li})_2(\text{P}_6\text{O}_{18})(\text{H}_2\text{O})_6$ is shown on **Fig. S7**. Six peaks with different intensities and line-widths are resolved, which correspond to the twelve crystallographically independent carbon atoms. Some peaks overlap due to the small chemical shift difference between them and the limited resolution power of the solid phase spectra.

The ^{15}N CP-MAS NMR spectrum of the title compound, shown in **Fig. S8**, is also in good agreement with the X-ray structure. Indeed, it exhibits two well-defined resonances at -361.9 and -364.2 ppm corresponding to the two crystallographically independent nitrogen atoms, in agreement with two organic cations in the unit cell.

Cyclohexaphosphates are formed by tetrahedra sharing two corners with neighboring tetrahedra (Q^2 units in Lipmaa's notation) [32], and two other ones interacting with cations.

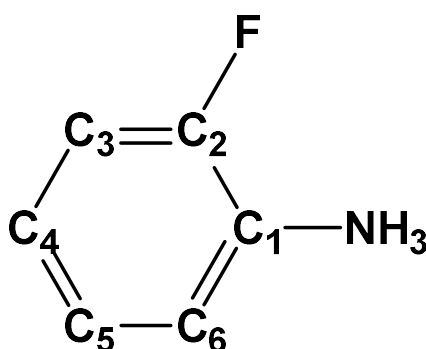
According to this, the ^{31}P isotropic chemical shift value δ_{iso} are higher than those corresponding to monophosphates (between -10 and +5 ppm) or diphosphates (between -10 and -20 ppm) of alkali and alkaline-earth cations [33-37]. Chemical shift values of cyclohexaphosphates are similar to those obtained previously in polyphosphates, indicating that δ_{iso} values are mainly defined by tetrahedral condensation of phosphates.

The solid state ^{31}P spectrum of the sample is formed by three species (**Fig. S9**) corresponding to the three crystallographically independent phosphorus atoms. As the chemical environments of all P-atoms are similar in the cyclohexaphosphate, resolved components must correspond to different crystallographic sites occupied by P-atoms. On the other hand, distortions of the PO_4 polyhedra are responsible for the observed chemical shift anisotropies and for the detection of numerous spinning sidebands. The spectral domain occupied by these sidebands is proportional to the tetrahedral distortions. Hence, NMR patterns could be used to detect minor distortions. To analyze this point, experimental envelopes were deconvoluted, determining for each component δ_{iso} , $\Delta\delta_{\text{CS}}$ and η (**Table S4**).

The solid state ^{19}F spectrum of the sample is formed by two components with their corresponding satellite spinning bands spaced at equal intervals (**Fig. S10**). This number of NMR components is consistent with the presence of two organic entities in the asymmetric unit of the compound as revealed by single crystal X-ray diffraction.

Theoretical calculations with Gaussian 09 were undertaken in order to assign the NMR resonances to the different crystallographic non-equivalent carbon atoms of the unit cell. The chemical shifts calculations were made on the organic molecules only. X-ray diffraction data give C-H or N-H distances which are too small compared to what is usually obtained by theoretical calculations or neutron diffraction (typically below 0.1 nm by X-ray instead of 0.109 nm for C-H and 0.105 nm for N-H) due to the fact that this method is not sensitive to the nuclei

but to the electrons and so gives values corresponding to distances between the barycenters of electronic charges. As a consequence, the positions of the hydrogen atoms were first optimized with the B3LYP/6-31+G* method, the other atoms being frozen. Then, the absolute chemical shifts of all atoms were calculated with Gaussian 09 using the GIAO method. Finally, the calculated values were calibrated relative to tetramethylsilane with $\delta_{\text{exp}} = 0$ ppm for carbon and Me_4P^+ at 24.4 ppm for phosphorus. The atoms of the organic molecule are labeled as depicted below:



Various calculations were made: (i) the two organic molecules separately (isolated ligands), (ii) a system with the two organic molecules in order to determine the presence or not of π - π interactions, (iii) the cyclophosphate alone, (iv) the cyclophosphate and the four Li^+ ions around it and finally (v) a full system containing the cyclophosphate, the two organic ligands and the four Li^+ cations (note that in that case the symmetry of the cyclophosphate was lost).

The results are listed on **Tables S5 and 6**. Clearly, there is a very good agreement between the experimental and the theoretical values, allowing unambiguously the assignment of the different NMR signals, even if the calculated values for the isotropic chemical shifts are sometimes far away from the experimental ones. The C2 carbon atom resonates as a doublet because of its coupling to the fluorine atom. The signal of the C1 carbon atom is not observed because this atom is not directly bonded to an hydrogen atom.

3.6. Electrochemical characterization

The ionic conductivity measurement was performed in air in the temperature range of 75 °C- 150 °C. A complex plane plot of real impedance, Z' , versus imaginary impedance, $-Z''$, was prepared for the set of data.

Impedance spectra measured between 75°C-150 °C under air with equivalent circuit is illustrated in **Fig. S11**. The data of the complex impedance spectra was fitted to the equivalent circuit of the R_s (R//CPE) type shown in **Fig. S11**, where R_s is the ohmic resistance of the $(C_6H_7FN)_4(Li)_2(P_6O_{18})(H_2O)_6$ pellet and the connected elements (R// CPE). R is resistance and CPE is a constant phase element representing time-dependent capacitive elements [38].

For the impedance spectra mentioned above, the conductivity can be obtained using the following equation:

$$\sigma = t/A \times 1/R$$

where t is the thickness of the sample and A is the electrode surface area. The ratio t/A is the sample's geometric factor. Activation energies (E_a) were calculated by fitting the conductivity data to the Arrhenius relation for thermally activated conduction, given by the following relation:

$$\sigma = \frac{\sigma_0}{T} \exp\left(-\frac{E_a}{kT}\right)$$

where σ , T , k , E_a and σ_0 are the conductivity, absolute temperature, Boltzmann constant, activation energy and a pre-exponential factor, respectively.

Fig. 5 shows the conductivity of the $(C_6H_7FN)_4(Li)_2(P_6O_{18})(H_2O)_6$ sample. It shows that the behavior of the samples is very similar to figures published by different authors [39, 40-44].

The calculated conductivity and activation energy of this composition were equal to $4.93 \times 10^{-4} \text{ Scm}^{-1}$ at 150 °C and 1.65 eV, respectively. Conductivity was higher than that found for the

lithium gadolinium polyphosphate [44] and also higher than what has been reported in the literature [42, 45]. Indeed, this value is larger than what has previously been found for numerous olivine-type-phase solid solutions, such as LiMPO_4 (M=Ni, Mn and Co) [43]. N. Bounar et al. [39] reported that the conductivity of the $\text{LiTi}_{2-x}\text{Sn}_x(\text{PO}_4)_3$ series synthesized by the solid state reaction was affected by the Sn^{3+} content. The ionic conductivity was of the order of 10^{-4} – 10^{-5} S cm^{-1} . Subsequently, S. Gao et al. [46] studied the effect of the B^{3+} amount on the ionic conductivity for $\text{Li}_x\text{B}_{1-x/3}\text{PO}_4$ compounds produced using a soft-chemistry route. Their studies revealed that the highest ionic conductivity was observed when the B content was 5% (3.35×10^{-5} S/cm at room temperature), which is lower than that for our sample, 3.67×10^{-5} S/cm. According to Vijayan et al. [39], the conductivity of the $\text{LiNi}_{1-x}\text{Mg}_x\text{PO}_4$ and $\text{LiNi}_{1-x}\text{Cu}_x\text{PO}_4$ series prepared by the citric acid assisted solution combustion technique was affected by the Mg^{2+} and Cu^{2+} content. The $\text{LiNi}_{0.9}\text{Mg}_{0.1}\text{PO}_4$ and $\text{LiNi}_{0.9}\text{Cu}_{0.1}\text{PO}_4$ compositions exhibit the highest conductivity.

3.7. Vibrational analysis

FT-IR spectroscopy was used to verify the functional groups present in the crystal and to investigate their vibrational behavior in the solid state. The IR spectrum of $(\text{C}_6\text{H}_7\text{FN})_4(\text{Li})_2(\text{P}_6\text{O}_{18})(\text{H}_2\text{O})_6$ recorded at room temperature is illustrated in **Fig. S12**. It shows the bands corresponding to vibrations of $(\text{P}_6\text{O}_{18})^{6-}$ anion OH groups and 2-fluoro-anilinium cation

According to the previous studies of cyclohexasilicates [47, 48] and based on some studies carried out for previous works [49-51] and reported on similar cyclohexaphosphates compounds [52], we propose an attempt of assignment of the observed bands. The stretching P-O modes of P_6O_{18} ring are observed in the following regions: 1350 – 1180 cm^{-1} for $\nu_{\text{as}}(\text{OPO})^-$, 1180 – 1060 cm^{-1} for $\nu_{\text{s}}(\text{OPO})^-$, 1060 – 960 cm^{-1} for $\nu_{\text{as}}(\text{POP})$ and 850 – 660 cm^{-1} for $\nu_{\text{s}}(\text{POP})$. [53,

54] For the title compound, characteristic bands at 1240 and 1081 cm^{-1} are related to asymmetric and symmetric stretching vibrations of OPO groups, while those at 968 and 763 cm^{-1} are assigned to POP groups (Fig. 5). Nevertheless special cautions must be paid in attribution of these bands because of their possible overlapping with the stretching $\nu(\text{C-C})$ and $\nu(\text{C-N})$, $\delta(\text{C-H})$ and $\gamma(\text{C-H})$ vibrations **[55]**. Frequencies below 660 cm^{-1} are attributed to bending, translation and rotation of the P_6O_{18} anion. C-C bending and NH_3 torsion may occur in this region.

The bands in the high-frequency region, between 3400 and 2500 cm^{-1} , correspond to the stretching vibrations of the N-H, C-H and O-H groups interconnected by a system of hydrogen bonds in the crystal **[56]**. The band at 1644 cm^{-1} corresponds to $\delta(\text{O-H})$ and $\delta(\text{N-H})$ deformation vibrations. The two bands at 1570 and 1500 cm^{-1} are assigned to $\nu(\text{C=C})_{\text{Ar}}$ stretching vibrations **[57, 58]**. The C-C stretching vibrations of aromatic groups usually occur as associated with other bands below 1650 cm^{-1} **[59]**.

Conclusion

The synthesis and characterization of the new organic cyclohexaphosphate, $(\text{C}_6\text{H}_7\text{FN})_4(\text{Li})_2(\text{P}_6\text{O}_{18})(\text{H}_2\text{O})_6$, has been described. The crystal packing is built by inorganic layers of $[\text{Li}_2\text{P}_6\text{O}_{18}\cdot\text{H}_2\text{O}]^{4-}$ hetero-anions and organic ones made by $[\text{C}_6\text{H}_7\text{N}]^+$ cations. The intermolecular cohesion is ensured by N-H...O, O-H...O, N-H...F and C-H...O hydrogen bonds. The enrichment ratio, derived from the Hirshfeld contact surface analysis, allows determining which types of contacts are over- or under-represented in crystal packing. Investigation of intermolecular interactions in the crystal packing reveals that the O...Hn/o intermolecular interactions are the most abundant contacts in the crystal packing and are significantly enriched. The C...C weak interactions are the most over-represented due to $\pi\cdots\pi$ stacking between the two 2-fluoroaniline rings. Weak interaction of hydrophobic nature

involving C, Hc and F atoms account for one quarter of contacts while contacts between the other more charged atoms represent half of the contact surface. The numbers of ^{13}C , ^{15}N , ^{31}P and ^{19}F CP-MAS NMR lines agree with the X-ray structure. DFT calculations allow the attribution of the NMR peaks to the independent crystallographic sites.

The obtained Electrochemical results show that the new $(\text{C}_6\text{H}_7\text{FN})_4(\text{Li})_2(\text{P}_6\text{O}_{18})(\text{H}_2\text{O})_6$ organic cyclohexaphosphate may be useful in a great variety of devices such as batteries, super-capacitors and gas sensors.

Supplementary data

Crystallographic data for the structural analysis have been deposited at the Cambridge Crystallographic Data Centre, CCDC No1816761. These data can be obtained free of charge via <http://www.ccdc.cam.ac.uk/conts/retrieving.html>, or from the CCDC, 12 Union Road, Cambridge, CB2 1EZ, UK: fax: (+44) 01223-336-033; e-mail: deposit@ccdc.cam.ac.

References

- [1] A. Assani, M. Saadi, M. Zriouil, L. El Ammari, *Acta Cryst.* E68 (2012) i30.
- [2] N. N. Chudinova, E. V. Murashova, B. S Zakharova, , *Zh. Neorg. Khim.* 43 (1998) 885-889.
- [3] *Lazernye Fosfatnye Stekla* (1980). In *Laser Phosphate Glasses*, Zhabotinskii M E (ed) (Moscow: Nauka)
- [4] A. Hamdi, L. Khederi, M. Rzaigui *Acta Cryst.* E70 (2014) o342-o343
- [5] R. Bel Haj Salah, L. Khederi, M. Rzaigui. *Acta Cryst.* E70 (2014).o61
- [6] R. Bel Haj Salah, L. Khedhiri, C. Ben Nasr, M. Rzaigui, F. Lefebvre. *Phosphorus, Sulfur, and Silicon*, 185 (2010) 595–601
- [7] L. Khedhiri, R. Bel Haj Salah, W. Belam, M. Rzaigui. *Acta. Cryst.* E63 (2007).o2269-o2271.

- [8] L. Khedhiri, S. Akriche, S. S. Al-Deyab, M. Rzaigui. *Acta Cryst.* E68 (2012) o2038–o2039
- [9] L. Khedhiri, A Selmi, M. Rzaigui. *J. Chem. Biochem.* 2 (2014), 179-192
- [10] I. Ameer, S. Abid, S. S. Al-Deyab, M. Rzaigui, *Acta Cryst.* E69 (2013) m305-m306
- [11] R. Bel Haj Salah, L. Khedhiri, M. Rzaigui, *X-Ray Struct. Anal. Online.* 26 (2010) 45-46.
- [12] L. Khedhiri, *X-Ray Struct. Anal. Online.* 20 (2004) x143-x144.
- [13] O. Amri, S. Abid, M. Rzaigui, *Phosphorus Sulfur Silicon Relat. Elem.*, 184, (2009) 766-777.
- [14] U. Schülke, R. Kayser. *Z. Anorg. Allg. Chem.* 531(1985) 167-175.
- [15] Bruker (2016). APEX3 suite. Bruker AXS Inc., Madison, Wisconsin, USA.
- [16] R. H. Blessing, *Direct Methods for Solving Macromolecular Structures*, *Acta Cryst.* A51 (1995) 33-38
- [17] A. Altomare, M. C. Burla, M. Camalli, G. L. Cascarano, C. Giacovazzo, A. Guagliardi, A. Grazia, G. Moliterni, G. Polidori, R. J. Spagna, *SIR97: a new tool for crystal structure determination and refinement*, *J. App. Cryst.* 32 (1999) 115-119.
- [18] G. M. Sheldrick, *SHELXTL Version 2014/7.* <http://shelx.uni-ac.gwdg.de/SHELX/index.php>.
- [19] Dolomanov, O.V.; Bourhis, L.J.; Gildea, R.J.; Howard, J.A.K.; Puschmann, H., *OLEX2: A complete structure solution, refinement and analysis program* (2009). *J. Appl. Cryst.*, 42, 339-341.
- [20] K. Brandenburg (1998). *Diamond Version 2.0 Impact GbR.* Bonn, Germany.
- [21] Bruker WINFIT Program' Bruker Rep. 140 (1994) 43-46.
- [22] J. Herzfeld, A. L. Berger, *J. Chem. Phys.* 73 (1980) 6021-6030.
- [23] W. Baur, *Acta Cryst.* B30 (1974) 1191-1195

- [24] L. Khedhiri, E. Jeanneau, F. Lefebvre, M. Rzaigui, C. Ben Nasr. *J. Mol. Struct.* 1105 (2016) 87-95
- [25] R. Fezai, A. Mezni, M. Kahlaoui, M. Rzaigui. *J. Mol. Struct.* 1119 (2016) 54-63
- [26] L. Khedhiri, E. Jeanneau, F. Lefebvre, M. Rzaigui, C. Ben Nasr. *J. Chem. Sci.* 128, (2016), 1037-1045
- [27] R. Fezai, H. Hemissi, A. Mezni, M. Rzaigui. *J. Mol. Struct.* 1150 (2017) 481-492
- [28] B. Guillot, E. Enrique, L. Huder, C. Jelsch, *Acta Cryst. A*70 (2014) C279
- [29] C. Jelsch, S. Soudani, C. Ben Nasr, *IUCr J.* 2 (2015) 327 - 340
- [30] M. J. Frisch, G. W. Trucks, H. B. Schlegel, G. E. Scuseria, M. A. Robb, J. R. Cheeseman, G. Scalmani, V. Barone, B. Mennucci, G. A. Petersson, H. Nakatsuji, M. Caricato, X. Li, H. P. Hratchian, A. F. Izmaylov, J. Bloino, G. Zheng, J. L. Sonnenberg, M. Hada, M. Ehara, K. Toyota, R. Fukuda, J. Hasegawa, M. Ishida, T. Nakajima, Y. Honda, O. Kitao, H. Nakai, T. Vreven, J. A. Montgomery, Jr., J. E. Peralta, F. Ogliaro, M. Bearpark, J. J. Heyd, E. Brothers, K. N. Kudin, V. N. Staroverov, R. Kobayashi, J. Normand, K. Raghavachari, A. Rendell, J. C. Burant, S. S. Iyengar, J. Tomasi, M. Cossi, N. Rega, J. M. Millam, M. Klene, J. E. Knox, J. B. Cross, V. Bakken, C. Adamo, J. Jaramillo, R. Gomperts, R. E. Stratmann, O. Yazyev, A. J. Austin, R. Cammi, C. Pomelli, J. W. Ochterski, R. L. Martin, K. Morokuma, V. G. Zakrzewski, G. A. Voth, P. Salvador, J. J. Dannenberg, S. Dapprich, A. D. Daniels, O. Farkas, J. B. Foresman, J. V. Ortiz, J. Cioslowski, and D. J. Fox, *Gaussian 09, Revision A.02*, Gaussian, Inc., Wallingford CT, 2009.
- [31] H. Saeidian, M. Sahandi, *J. Mol. Struct.* 1100 (2015) 486-495.
- [32] E. Lippmaa, M. Magi, A. Samoson, M. Tarmak, G. Engelhardt, A. R. Grimmer, *J. Am. Chem. Soc.*, 102 (1980) 4889-4893.

- [33] A. R. Grimmer, U. Haubenreisser, *Chem. Phys. Lett.* 99 (1983) 487-490.
- [34] D. Müller, E. Jahn, G. Ladwig, U. Haubenreisser, *Chem. Phys. Lett.* 109 (1984) 332-336.
- [35] S. Prabhakar, K. J. Rao, C. N. R. Rao, *Chem. Phys. Lett.* 139 (1987) 96-102.
- [36] P. Hartmann, J. Vogel, B. Schnabel, *J. Magn. Reson. A* 111 (1994) 110-114.
- [37] L. Mudrakovskii, V. P. Shmochkova, N. S. Kotsarenko, V. M. Mastikhin, *J. Phys. Chem. Solids*, 47 (1986) 335-339.
- [38] M. Kahlaoui, A. Inoubli, S. Chefi, A. Mezni, A. Kouki, A. Madani, C. Chefi, *J. of hyd. Energy*. 41 (2016) 4751–4764.
- [39] L. Vijayan, R. Cheruku, G. Govindaraj, *Mater Res Bull* 50 (2014) 341–347.
- [40] S. Geng, Y. Yang, Y. Zhang, W. Ding, X. Wang, H. Peng, Z. Bakenov, *Electrochim Acta* 176 (2015) 327–333.
- [41] S. V. Pershina, A. A. Raskovalov, B. D. Antonov, T. V. Yaroslavtseva, O. G. Reznitskikh, Ya. V. Baklanova, E. D. Pletneva, *J Non-Cryst Solids* 430 (2015) 64–72.
- [42] L. Le Van-Jodin, F. Ducroquet, F. Sabary, I. Chevalier, *Solid State Ionics* 253 (2013) 151–156.
- [43] R. Cheruku, G. Kruthika, G. Govindaraj, L. Vijayan, *J Phys Chem Solids* 86 (2015) 27–35.
- [44] H. Ettis, H. Naïli, T. Mhiri, *J Solid State Chem* 179 (2006) 3107–3113.
- [45] M. Ferhi, K. Horchani-Naifer, Kh. Ben Saad, M. Férid, *Physica B* 407 (2012) 2593–2600.
- [46] S. Gao, M. Shui, W. Zheng, T. Yang, J. Shu, L. Cheng, L. Feng, Y. Ren, *Mater Res Bull* 48 (2013) 2896–2900.
- [47] E. Sterger, *Z. Anorg. all. Chem.* (1958) 294 146-154.
- [48] F. Matossi, *J. Chem. Phys.* (1949) 17 679-685.

- [49] Kh. Kh. Mulglaiev, A. N. Lazarev, A. P. Mirgodsku. *Izv. Acad. Nauk. SSSR Neorg. Mater.* (1974) 10 563
- [50] E. Sterger, A. Simon, *Z. anorg. all. Chem.* (1957) 291 76-88.
- [51] A.N. Lazarev, *Opt. Spectrosc.* (1968) 12 28.
- [52] A. Gharbi, A. Jouini and A. Durif, *J Solid State Chem.* 114 (1995) 42-51
- [53] K. Kamel, A. Rayes, C. Ben Nasr, M. Rzaigui, F. Lefebvre, *Mater. Res. Bull.*, 38 (2003) 741-747
- [54] A. Oueslati, C. Ben Nasr, A. Durif, F. Lefebvre, *Mater. Res. Bull.* 40 (2005) 970-980
- [55] C. Ben Nasr, *Solid State Sci.* 2 (2000) 501-506
- [56] W. Clegg, D. G. Watson, *Acta Cryst.* E63 (2007) o929-o931
- [57] C. Ben Nasr, M. Rzaigui, *Mater. Res. Bull.* 34 (1999) 557-569.
- [58] S. Soudani, J.-X. Mi, F. Lefebvre, C. Jelsch, C. Ben Nasr, *J. of Mol. Struct.* 1084 (2015) 46-54.
- [59] E. Temel, C. Alaşalvar, H. Gökçe, A. Güder, Ç. Albayrak, Y.B. Alpaslan, G. Alpaslan, *Spectrochim. Acta A* 136 (2015) 534-546.

Fig. 1 ORTEP view of (**I**). Displacement ellipsoids are drawn at the 40% probability level and H atoms are shown as small spheres of arbitrary radii. [Symmetry codes: (i) $x+1, y, z$, (iii) $-x, 1-y, 1-z$, (vi) $-x-1, -y, 1-z$]

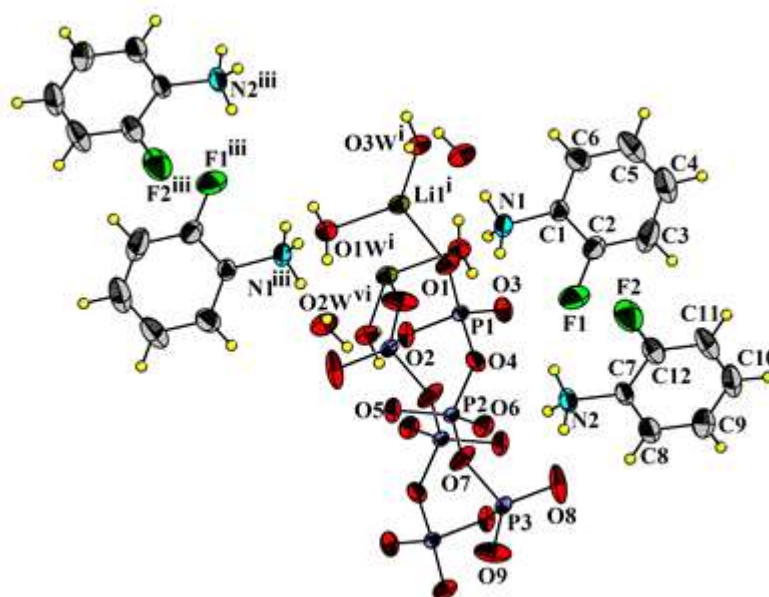


Fig. 2

Atomic arrangement of the title compound projected along the *a*-axis.

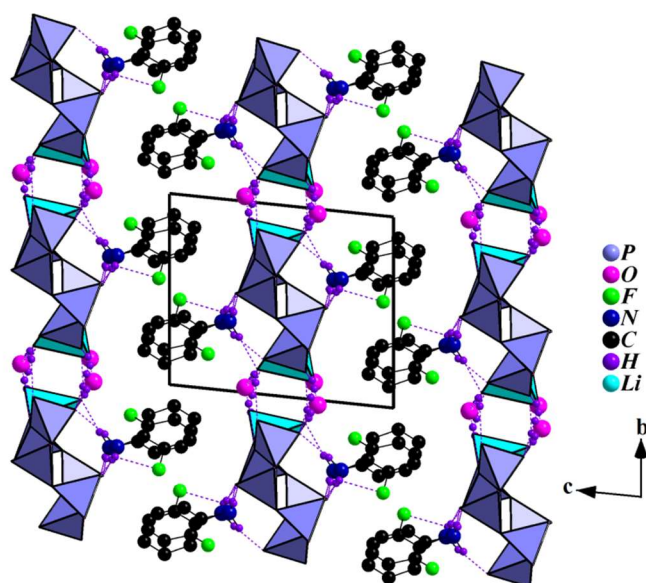


Fig. 3 Hirshfeld surface around the cyclohexaphosphate moiety along with an interacting fluoroaniline cation. (a) colored according inner atoms, oxygen: red, phosphorus: yellow.

(b) colored according to O...X contact.

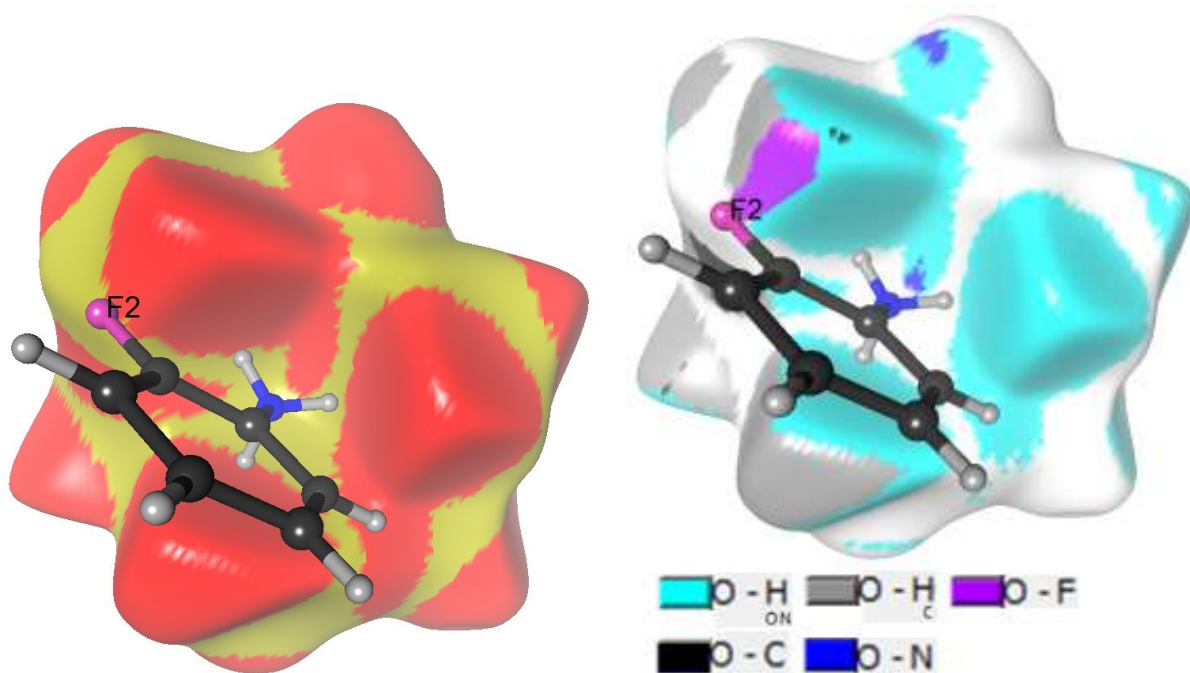


Fig. 4

Molecular Electrostatic Potential maps of the title compound.

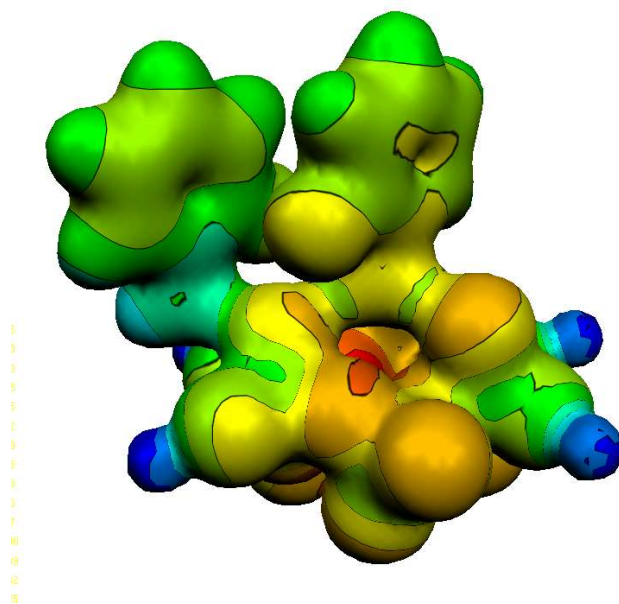


Fig. 5

Arrhenius plots and activation energies of $(C_6H_7FN)_4(Li)_2(P_6O_{18})(H_2O)_6$ sample.

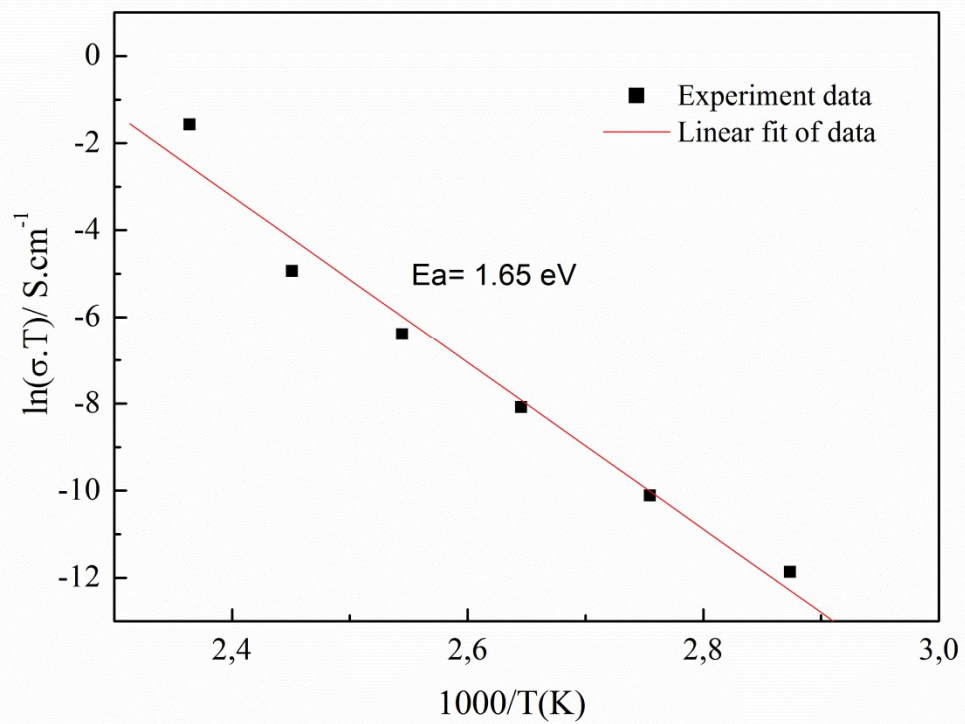


Table 1. The crystal data and experimental parameters used for the intensity data collection. Procedure and final results of the structure determination.

| | |
|--|--|
| Empirical formula | C ₂₄ H ₄₀ F ₄ Li ₂ N ₄ O ₂₄ P ₆ |
| Formula weight [g mol ⁻¹] | 522.15 |
| Crystal color, habit | pink, block |
| Crystal temperature [K] | 293(2) |
| Crystal size [mm ³] | 0.204 × 0.306 × 0.463 |
| Radiation, wavelength [Å] | MoK α , 0.71073 |
| Crystal system | triclinic |
| Space group | P-1 |
| Unit-cell dimensions: | |
| <i>a</i> , <i>b</i> , <i>c</i> [Å] | 9.839(8), 10.715(8), 11.344(9) |
| α , β , γ [°] | 83.75(3), 88.00(3), 63.82(3) |
| Volume [Å ³] | 1066.8(15) |
| <i>Z</i> | 2 |
| Density calc. [g cm ⁻³] | 1.626 |
| Reflections for cell determination | 25 |
| θ range for unit cell determination [°] | 8-10 |
| Absorption coefficient μ [mm ⁻¹] | 0.359 |
| <i>F</i> (000) | 536 |
| θ -Range for data collection [°] | 2.307 to 30.875 |
| Limiting indices | -14 ≤ <i>h</i> ≤ 13, -15 ≤ <i>k</i> ≤ 15, -16 ≤ <i>l</i> ≤ 16 |
| Reflections collected/unique | 48403/5642 (<i>R</i> _{int} = 0.03) |
| Refinement method | Full-matrix least-squares on <i>F</i> ² |
| Data, restraints, parameters (<i>I</i> > 2 σ) | 6517, 0, 337 |
| Goodness-of-fit on <i>F</i> ² | 1.025 |
| <i>R</i> indices (all data, on <i>F</i> ²) | <i>R</i> = 0.0520, <i>wR</i> = 0.1110 |
| $\Delta\rho$ (min, max) [e Å ⁻³] | -0.669 and 0.961 |

Table 2. Selected bond lengths (Å) and bond angles (°) in the organic groups.

| [C₆H₇FN(1)]⁺ group | | | |
|--|----------|-----------------|----------|
| F1 - C2 | 1.370(3) | C2 - C1 - C6 | 120.6(2) |
| N1 - C1 | 1.438(3) | C2 - C1 - N1 | 118.6(2) |
| C1 - C2 | 1.373(3) | C6 - C1 - N1 | 120.8(2) |
| C1 - C6 | 1.398(3) | F1 - C2 - C1 | 118.7(2) |
| C2 - C3 | 1.375(4) | F1 - C2 - C3 | 121.0(3) |
| C6 - C5 | 1.367(4) | C1 - C2 - C3 | 120.3(3) |
| C3 - C4 | 1.381(5) | C5 - C6 - C1 | 119.3(3) |
| C4 - C5 | 1.371(5) | C2 - C3 - C4 | 118.3(3) |
| | | C5 - C4 - C3 | 122.3(3) |
| | | C6 - C5 - C4 | 119.3(3) |
| | | | |
| [C₆H₇FN(2)]⁺ group | | | |
| F2 - C12 | 1.349(3) | C12 - C7 - C8 | 119.9(2) |
| N2 - C7 | 1.449(3) | C12 - C7 - N2 | 119.4(2) |
| C7 - C12 | 1.382(3) | C8 - C7 - N2 | 120.7(2) |
| C7 - C8 | 1.389(4) | F2 - C12 - C11 | 119.4(2) |
| C12 - C11 | 1.369(4) | F2 - C12 - C7 | 119.2(2) |
| C8 - C9 | 1.376(4) | C11 - C12 - C7 | 121.4(3) |
| C9 - C10 | 1.377(5) | C9 - C8 - C7 | 119.0(3) |
| C11 - C10 | 1.377(5) | C8 - C9 - C10 | 119.9(3) |
| | | C12 - C11 - C10 | 118.0(3) |
| | | C11 - C10 - C9 | 121.7(3) |

Table 3. Chemical proportions on the Hirshfeld surface, % contact types and their enrichment ratios. N chemical species, whose content is negligible on the surface, was omitted. The major interaction types and the most enriched are in bold. The hydrogen atoms (Ho/n and, Hc) bound to O/N and C are distinguished, as their electrostatic properties are different.

| atom | Ho/n | Li | O | P | F | C | Hc |
|-----------|-------------|-------------|------------|------|-------------|-----------------------|------|
| Surface % | 23.8 | 9.2 | 16.1 | 22.2 | 5.3 | 6.6 | 16.6 |
| Ho/n | 1.9 | | | | | | |
| Li | 4.6 | 0.0 | | | | contacts | (%) |
| O | 23.2 | 10.2 | 0.1 | | | <i>C_{xy}</i> | |
| P | 8.1 | 2.3 | 0.0 | 0.0 | | | |
| F | 2.3 | 0.2 | 0.5 | 0.1 | 0.0 | | |
| C | 1.3 | 0.3 | 0.7 | 0.6 | 4.2 | 8.4 | |
| Hc | 4.3 | 0.9 | 9.6 | 2.2 | 3.4 | 8.3 | 2.3 |
| Ho/n | 0.33 | | | | | | |
| Li | 1.02 | 0.00 | | | | <i>E_{xy}</i> | |
| O | 2.20 | 2.41 | 0.01 | | | | |
| P | 2.58 | 1.77 | 0.01 | 0.00 | | | |
| F | 0.90 | 0.19 | 0.22 | 0.08 | 0.00 | | |
| C | 0.18 | 0.10 | 0.10 | 0.26 | 2.47 | 3.25 | |
| Hc | 0.54 | 0.28 | 1.30 | 1.01 | 1.91 | 1.55 | 0.84 |